Praseodymium oxide improving the activity of silver loaded calcium titanate photocatalyst for carbon dioxide reduction with water

Hongxuan Qiu,[a] Akihiko Anzai,[a] Tayyebeh Soltani,[a] Akira Yamamoto,[a,b] Eri Fudo,[c] Atsuhiro Tanaka,[d,e] Hiroshi Kominami,[d] and Hisao Yoshida[a,b*]

[a] *Kyoto University, Graduate School of Human and Environmental Studies, Kyoto 606-8501, Japan*

[b] *Kyoto University, Elements Strategy Initiative for Catalysts and Batteries (ESICB), Kyoto 615-8520, Japan*

[c] *Molecular and Material Engineering, Interdisciplinary Graduate School of Science and Engineering, Kindai University, 3-4-1 Kowakae, Higashiosaka, Osaka 577-8502, Japan.*

[d] *Department of Applied Chemistry, Faculty of Science and Engineering, Kindai University, 3-4-1 Kowakae, Higashiosaka, Osaka 577-8502, Japan*

[e] *Precursory Research for Embryonic Science and Technology (PRESTO), Japan Science and Technology Agency (JST), 4-1-8 Honcho, Kawaguchi 332-0012, Japan*

* yoshida.hisao.2a@kyoto-u.ac.jp

Abstract

Heterogeneous photocatalytic CO_2 reduction with water has attracted great attentions. Although the addition of Ag nanoparticles (NPs) as a cocatalyst on the semiconductor photocatalyst has known to improve both the photocatalytic activity and the reaction selectivity for CO_2 reduction, the addition of praseodymium as Pr_6O_{11} species on the surface of Ag loaded $CaTiO_3$ (CTO) photocatalyst further improved the photocatalytic activity. The different calcination temperatures for the sample preparation changed the state of Pr species, and it strongly influenced the photocatalytic performance. The Pr_6O_{11} species was found to be loaded between the CTO surface and Ag NPs on the Ag/Pr/CTO photocatalyst, proposing that it improves the electron migration from the CTO photocatalyst to Ag NPs via the Pr_6O_{11} layer.

Keywords: Photocatalytic CO_2 reduction, CO formation, calcium titanate photocatalyst, different calcination temperatures, Ag cocatalyst, Pr_6O_{11}

1. Introduction

The rising level of carbon dioxide (CO_2) in the atmosphere has currently considered as the main causes of the greenhouse effect. The conversion of CO_2 into valuable compounds, such as CO and CH_4 by artificial photosynthesis has become a new research focus. [1-6] Industrially, carbon monoxide (CO) is the basis of one-carbon chemistry, mainly used for the production of methanol, phosgene, and organic synthesis.[7] Till date, a growing number of researchers have centered on photocatalytic CO_2 reduction with H_2O as a donor of electron to produce CO, since this system successfully takes the advantage of solar energy to convert CO_2 at mild conditions and the solar energy is converted to the chemical potential of the storable products.[8-9] In this photocatalytic reaction system, the reduction of CO_2 (eq. 1) and proton (eq. 2) can take place competitively with the common oxidation of H_2O (eq. 3). It is noted that the latter in the reduction reactions is more thermodynamically preferential than the former because the redox potential of H_2/H^+(−0.41 V vs NHE, pH=7) is more positive than that of CO/CO_2 (−0.53 V vs NHE, pH=7),[10] where the selective reduction of CO_2 into CO is essentially tough in an aqueous solution.

$$CO_2 + 2H^+ + 2e^- \rightarrow CO + H_2O \quad (1)$$

$$2H^+ + 2e^- \rightarrow H_2 \quad (2)$$

$$H_2O + 2h^+ \rightarrow 1/2O_2 + 2H^+ \quad (3)$$

In recent studies for the selective photocatalytic reduction of CO_2 by H_2O, many photocatalysts with the aid of silver cocatalyst have been reported such as $Ag/BaLa_4Ti_4O_{15}$,[11] Ag/Ga_2O_3,[12] $Ag/SrNb_2O_6$[13] and so on. However, there are still several challenges. For example, the recombination of photogenerated electron-hole pairs tends to take place rapidly and the CO production rate was very slow. Utilization of intermediate materials to transfer electrons between the photocatalyst surface and the Ag cocatalyst is likely to be one of the possible approaches to reduce the probability of recombination, which has been investigated in several systems such as Ag-BiOI-rGO,[14] Ag/CuO/ZnO,[15] and $Ag@AgVO_3$/BiOCl[16] in the field of photocatalytic degradation. Hence, this concept might be also applicable for the photocatalytic CO_2 reduction.

Among all rare earth elements, the limited elements such as cerium, terbium and praseodymium are allowed to be both tri- and tetravalent states.[17] This kind of elements possibly have a redox property, which can be beneficial for the electron transfer. Among them, only praseodymium has various oxide forms, such as PrO_2, Pr_2O_3, and Pr_6O_{11}.[18] At the ambient temperature and pressure, the most stable oxide substance is Pr_6O_{11} consisting of both Pr(III) and Pr(IV).[19] It has been applied for photodegradation[20-22] and humidity-independent gas sensors.[23] Recently, another property of praseodymium was also reported; Pr(III) species added on Ag/Ga_2O_3 photocatalyst can accumulate CO_2 in aqueous media to enhance the photocatalytic CO_2 reduction rate, where Pr(III) species existed as Pr hydroxycarbonates such as $Pr_2(OH)_{2(3-x)}(CO_3)_x$ and Pr carbonate hydrates ($Pr_2(CO_3)_3{\cdot}8H_2O$).[24] There are some cases that the state and the function of additives on the catalyst surface are determined by the property of the material.[1, 25-26]

In the present study, $CaTiO_3$ was used as a photocatalyst showing the high selectivity for both reaction selectivity and product selectivity with the assistant of Ag NPs cocatalyst, i.e., selective CO_2 reduction by H_2O in an aqueous media and selective CO formation as a product,[27] and Pr_6O_{11} was employed to modify the CTO surface. As a result, we found that the modified CTO photocatalyst exhibited high photocatalytic performance for CO_2 reduction to CO and it is proposed that the $Pr(III,IV)_6O_{11}$ layer located between the CTO surface and the Ag NPs cocatalyst enhances the electron transfer as an intermediate species.

Experimental section

1.1. Preparation of samples

Calcium titanate ($CaTiO_3$, CTO) sample was prepared by a flux method as our previous work[28] from $CaCO_3$ (Nacalai tesque, Inc. 99.5%) and rutile TiO_2 (High purity Chemical Co., Ltd, 99.9%) as precursors, where the molar ratio of $CaCO_3$ to TiO_2 was 1:1. After physical grinding these precursors for 20 min with 5 mL of ethanol in an aluminum mortar, NaCl was added as a flux in a 1:1 ratio of $CaTiO_3$ to NaCl, followed by heating at a rate of 200 K h^{-1} up to 1473 K and keeping this temperature for 10 h. The molten mixture was then cooled at a rate of 100 K h^{-1} to 773 K, followed by being naturally cooled to room temperature in the furnace. The obtained powder was thoroughly washed with hot water (500 mL, 353 K) for 15 min 3 times to remove residual flux, filtrated with suction, and dried at 323 K for 24 h, which provided the bare CTO sample.

Pr-modified $CaTiO_3$ samples were prepared by an impregnation method. 1.0 g of the CTO sample was introduced into an aqueous solution (100 mL) of desired amounts of $Pr(NO_3)_3$ (Kishida Chemical Co., Ltd, 99.5 %) with stirring in a beaker, heated at 353 K to evaporate water, dried at 373 K for 24 h, and finally calcined at 573, 773, 973 or 1223 K for 2 h in an electrical muffle furnace. The samples were referred to as Pr(*y*,*z*)/CTO, where *y* is the amount of Pr (wt%) and *z* is the calcination temperature (K).

The Ag cocatalyst was loaded by a photodeposition method. The prepared CTO or Pr(*y*,*z*)/CTO samples (1.0 g) were dispersed into 1.5 L of ion-exchanged water containing a required amount of $AgNO_3$ (Kishida Chemical Co., Ltd.) as a precursor with a bubbling flow of Ar for 2 h in dark conditions to purge out the air was completely. Then the suspension was photoirradiated by a 400 W high-pressure mercury lamp located at the center of the vessel. The samples were referred to as Ag(*x*)/CTO or Ag(*x*)/Pr(*y*,*z*)/CTO, where *x* is the amount of Ag (wt%).

For comparison, the bare CTO sample prepared by the flux method without loading any species were further calcined at various temperatures at 573, 773, 973 or 1223 K for 2 h, which gave the samples shown as CTO(*z*). The Ag cocatalyst was loaded by the photodeposition method, which were referred to as Ag(*x*)/CTO(*z*).

1.2. Characterization

The crystal structure of each sample was determined by X-ray diffraction pattern (XRD) with a Lab X XRD-6000 (Shimazu). Morphology of the samples was observed by scanning electron microscopy (SEM) with a JSM-890 (JEOL). The elemental analysis of the samples was observed by a field-emission scanning electron microscopy (SEM; SU-8220, Hitachi, Japan), augmented by energy dispersive X-ray spectroscopy (EDS, 15.0 kV). Diffuse reflectance (DR) UV-vis spectrum was measured with a V-570 (JASCO) and a $BaSO_4$ plate was used for the reference. For comparison of UV-vis spectra, pure Pr_6O_{11} (Wako Chemical Co., Ltd, 99.9%) was diluted with $BaSO_4$ (Nacalai tesque, Inc. 99.5%) by a factor of 100 times by weight[29] and measured as with the case of the samples.

Ag K-edge X-ray absorption fine structures (XAFS) were recorded at BL01B1 of SPring-8 in a transmission mode (Hyogo, Japan). The actual loading amount of Ag cocatalysts was measured by X-ray fluorescence (XRF) with an EDX-8000 (Shimadzu). The Brunauer-Emmett-Teller (BET) specific surface area was evaluated with a Monosorb (Quantachrome) at 77 K. Transmission electron microscopy (TEM) and scanning transmission electron microscopy (STEM) with energy dispersive X-ray analysis (EDX) were given with a JEOL JEM-2100F at 200 kV in the Joint Research Center of Kindai University. X-ray photoelectron spectroscopy (XPS) measurements were conducted using an

ESCA 3400 instrument (Shimadzu Corp.).

1.3. Photocatalytic reaction test

The photocatalytic activity test for CO_2 reduction with H_2O was carried out using a bubbling-flow system with an inner-irradiation reaction vessel by using a 400 W high-pressure mercury lamp.[30] The photocatalyst (0.3 g) was dispersed in ion-exchanged water (1.5 L) containing 1.0 M $NaHCO_3$ (Nacalai tesque, Inc.), and then magnetically stirring in a bubbling flow of CO_2 at a flow rate of 30 mL min^{-1} without irradiation for 2.0 h. After staring photoirradiation, the reaction temperature measured was 290 K. The products in the outlet gas were sampled at each scheduled time and analyzed by using an on-line gas chromatograph (Shimadzu, GC-8A, TCD, Shincarbon ST column, argon carrier). The main products under photoirradiation were CO, H_2 and O_2. Since the reduction products are limited to CO and H_2, the selectivity of CO (S_{CO}) is defined as shown in eq. 4. The ratio of the consumed electrons and holes was calculated by eq. 5.

$$S_{CO}(\%)=R_{CO}\times 100/(R_{CO}+R_{H_2}) \quad (4)$$

$$R\ (e^-/h^+)=(R_{CO}+R_{H_2})/2R_{O_2} \quad (5)$$

where R_{CO}, R_{H_2} and R_{O_2} are the formation rate of CO, H_2 and O_2, respectively.

The resulting solution after the reaction was mixed with the same volume of pure decane (Nacalai tesque, Inc.), and then was analyzed by GC-MS (Shimadzu, GCMS-QP2020). The analysis was carried out without neutralization.

To check the reusability of the optimal photocatalyst, the one used for the reaction test was collected by filtration and dried at 353 K overnight, and then applied again for the photocatalytic CO_2 reduction in the same procedure as mentioned above.

In the O_2 evolution test, the bare CTO and Pr(1.0,773)/CTO samples were prepared and examined in the reactor containing ion-exchanged water (1.5 L) with the presence of $NaIO_3$ (5 mM, Nacalai tesque, Inc.) solution as a sacrificial oxidant.

2. Results and discussion

2.1. Characterization of the samples

The crystal structure of the bare CTO and Pr-modified CTO samples was investigated by XRD (Fig. 1A). The diffraction patterns of the bare CTO sample (Fig. 1Aa) coincided with that of the $CaTiO_3$ with a perovskite structure (ICSD# 162909)[31] and no other impurity phase was observed. In the Pr-modified CTO samples calcined at 573 K, no change was observed from the bare CTO sample (Fig. 1A,c–e). In contrast, a broad diffraction line of Pr_6O_{11} (ICSD# 82107)[32] appeared for the Pr(1.0,*z*)/$CaTiO_3$ samples of the calcination temperature over 773 K (Fig. 1B,c–e) without changing the structure of $CaTiO_3$ (Fig. 1A,c–e). It was reported that the Pr nitrate hydrates started to decompose via multi-step processes and form praseodymium oxide, Pr_6O_{11}, consisting of both Pr(III) and Pr(IV), over 738 K.[33] The decomposition temperature coincided with the XRD results that the Pr_6O_{11} species was formed over 773 K. In literature, XRD patterns revealed that Pr species on Ga_2O_3 photocatalyst surface formed $Pr_2O_2CO_3$ and $Pr(OH)_3$ phases even though calcined at 1223 K,[24] whose phases were not observed and instead Pr_6O_{11} phase was confirmed in the present case.

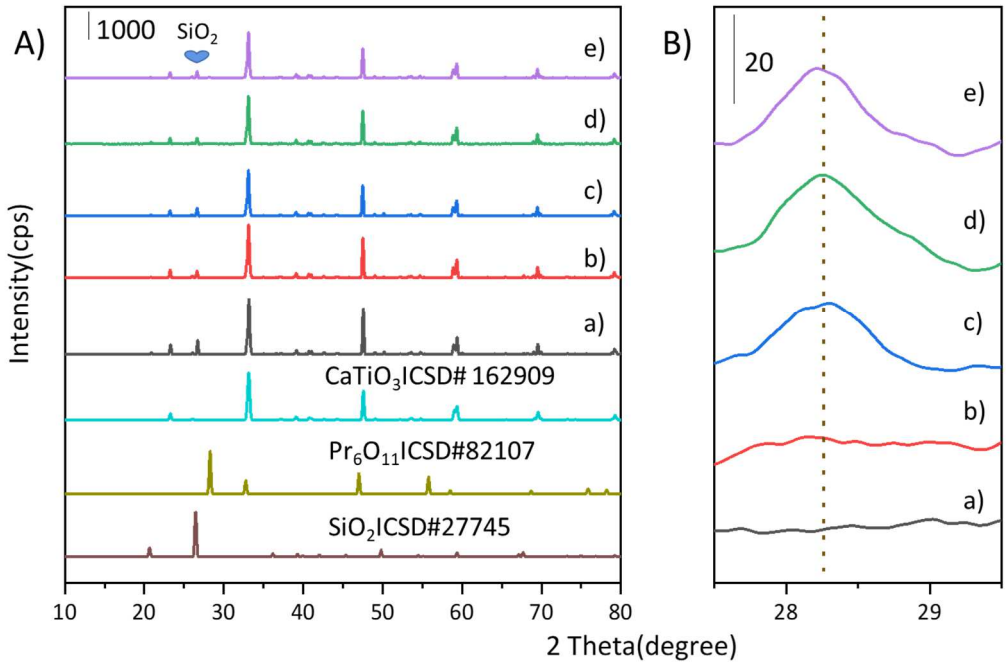

Fig. 1. [A] XRD patterns of (a) the bare CTO sample, and various samples of Pr(1.0,*z*)/CTO, where *z* K was (b) 573, (c) 773, (d) 973, and (e) 1223 as well as the ICSD reference data for Pr_6O_{11}, $CaTiO_3$ and SiO_2 (quartz), where SiO_2 was used for angle calibration. **[B]** The magnified regions showing the diffraction line of Pr_6O_{11} (111). The angle was corrected according to a diffraction of SiO_2 powder mixed with each sample.

The DR UV-vis spectra of these samples with different calcination temperatures are shown in Fig. 2A. The spectrum of the bare CTO sample showed a large absorbance in the range of shorter wavelength less than 350 nm and a broad and weak absorption band centered around 500 nm, which are assignable to the excitation from valence band to conduction band and defects of $CaTiO_3$, respectively.[17, 34] The Pr(1.0,573)/CTO (Fig.2Ab) sample showed no significant peak assignable to the Pr species although the absorption band around 500 nm was slightly decreased, implying the surface defects of $CaTiO_3$ were decreased by loading Pr species and calcining at 573 K. On the other hand, calcination at higher temperatures over 573 K ($z > 573$ K) provided a broad absorption band at 360–600 nm (Fig. 2A,c–e), and the band intensity was enhanced with increasing calcination temperature. Separately, we confirmed that the DR UV-vis spectrum of the pure Pr_6O_{11} diluted by 100 times in weight (Fig. S1) has an absorption band centered around 500 nm, which exhibits almost similar absorption intensity to the Pr/CTO samples. This means that the formation of Pr_6O_{11}, which is confirmed by XRD, increased the absorption band around 360–600 nm in the UV-vis spectra of the Pr(*y*,*z*)/CTO samples. In addition, the change of the band shape and intensity was also observed when the sample was calcined at more than 573 K, suggesting that the state of Pr_6O_{11} was changed by increasing the calcination temperature and the calcination at 573 K was not enough high to form the Pr_6O_{11} species. After loading Ag cocatalyst by the PD method, absorption at 350–800 nm increased, it is due to the formation of Ag NPs in the Ag(3.5)/Pr(1.0, $z \geq 773$ K)/CTO samples (Fig. 2Bf–g). It was also confirmed that the absorption property of Ag NPs was influenced

by the calcination temperature of the Pr/CTO samples.

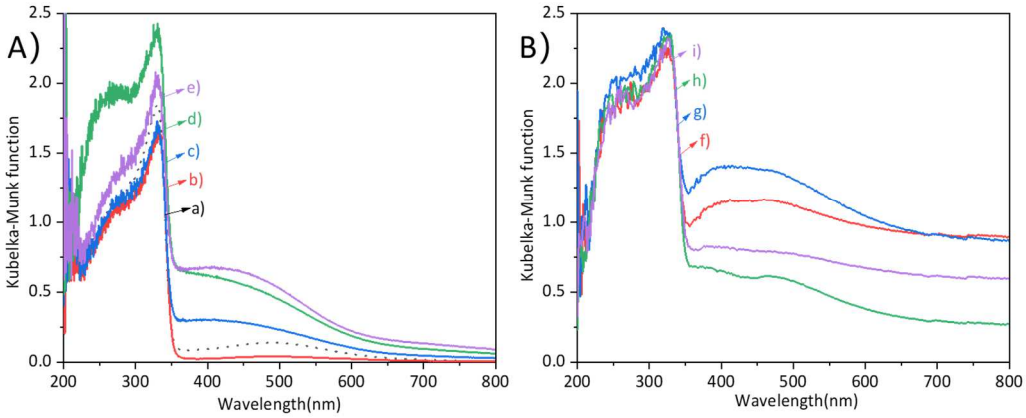

Fig. 2. DR UV-vis spectra of **[A]** (a) the bare CTO sample (dotted line) and the Pr(1.0,*z*)/CTO samples (solid lines), where *z* K was (b) 573, (c) 773, (d) 973, and (e) 1223 and **[B]** the Ag(3.5)/Pr(1.0,*z*)/CTO samples, where *z* K was (f) 573, (g) 773, (h) 973, and (i) 1223.

The XPS spectra was performed to examine the chemical composition about the surface of representative samples (Fig. 3). Through the surface-measurement analysis (Fig. 3A), it is good evidence for the existence of PrO_x with tri/tetravalent states, which is indicative of the peaks at 929.5 and 948.4 eV assigned to Pr(III) and other peaks at 934.9 and 954.3 eV for Pr(IV).[23, 35-36] From the Table 1, the peak intensity of Pr^{3+} increases along with increasing calcination temperature, suggesting that more Pr^{4+} is reduced to Pr^{3+}.[37] The XPS record of Ca 2p region shows two peaks for Ca $2p_{1/2}$ and Ca $2p_{3/2}$ at bonding energies of 350.7 and 347.2 eV, respectively (Fig. 3B).[38] The high calcination temperature made the CTO with position of Ca peaks to shift around 0.2 eV, which attributed to the dopant of Pr. Although the XRD line position of the CTO sample was not shifted clearly by increasing the calcination temperature (Fig. 1a); Pr doping would possible result from the similar ionic radii of Pr^{3+} (1.30 Å, CN = 12) and Ca^{2+} (1.34 Å, CN = 12).[39] The other trivalent lanthanoids can substitute Ca^{2+} of the A-site of $CaTiO_3$ perovskite based on the previous reports.[34, 40-41] All samples contain similar two bands from Ti^{4+} peaks at 458.9 eV ($2p_{3/2}$) and 464.9 eV ($2p_{1/2}$) (Fig. 3C),[38] indicating that high calcination temperature did not affect the nature of Ti species. Similarly, the spectra of Ag (Fig. 3D) on the surface have no huge difference with two peaks at 368.3 and 374.3 eV, corresponding to the Ag $3d_{5/2}$ and Ag $3d_{3/2}$, respectively.[42]

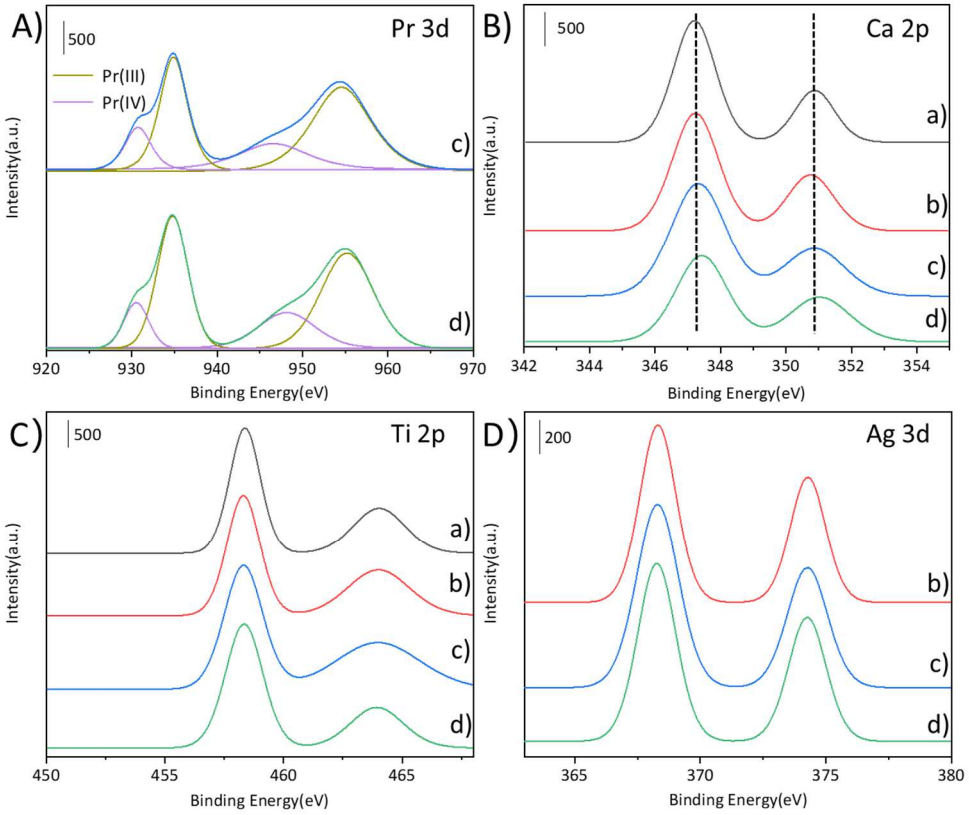

Fig. 3. XPS spectra for **[A]** Pr 3d, **[B]** Ca 2p, **[C]** Ti 2p, and **[D]** Ag 3d of (a) the bare CTO sample, (b) the Ag(3.5)/CTO sample, (c) the Ag(3.5)/Pr(1.0,773)/CTO sample, and (d) the Ag(3.5)/Pr(1.0,1223)/CTO sample.

Table 1 The Atomic % of Pr(III) and Pr(IV) estimated by XPS

The name of sample	Atmoic %	
	Pr(III)	Pr(IV)
Ag(3.5)/Pr(1.0,773)/CTO	26.0	74.0
Ag(3.5)/Pr(1.0,1223)/CTO	30.1	69.9

Fig. 4 shows the SEM images of the bare CTO sample, and the Pr(1.0,*z*)/CTO samples. Although the crystal morphology of the CTO sample was not changed significantly when Pr was loaded and calcined at less than 773 K (Fig. 4a–c), increasing the calcination temperature ($z \leq 773$) in the presence of the Pr species decreased the average particle size of CTO (Fig. S2a–c) and lowered the BET specific surface area (Table S1). Calcination without Pr addition did not change the particle size of CTO (Fig. S2e, f) and the specific surface area (Table S1). From SEM-EDS (Fig. S3A) and STEM-elemental analysis (Fig. S4), it can be seen that Pr species in the sample calcined at 773K formed surface layers or granular substances, which were randomly distributed on the surface of CTO. Meanwhile, we confirmed the increased fragments of the particles possibly assignable to the Pr species formed at 773 K in enlarged images (Fig. S5a, c). On the other hand, it is evident for dopant of Pr (Fig. S3B) that the calcination at 1223 K made the Pr species uniformly covered the CTO

without the clear particles for Pr species. Therefore, the high-temperature calcination at 1223 K drastically changed the morphology of the particles (Fig. 4d), while calcination of the bare CTO sample at 1223 K did not change its morphology (Fig. S5f). These results strongly suggest that loading Pr species changed the morphology and reduced the particle size only at the high calcination temperature such as 1223 K (Fig. 4d and S5g). The Pr would be doped into the CTO lattice at high temperature to change the original CTO particles to smaller particles. Thus, this variation in morphology (Fig. S5g) would presumably result from the Pr doping based on an analogy with the other lanthanides.[43]

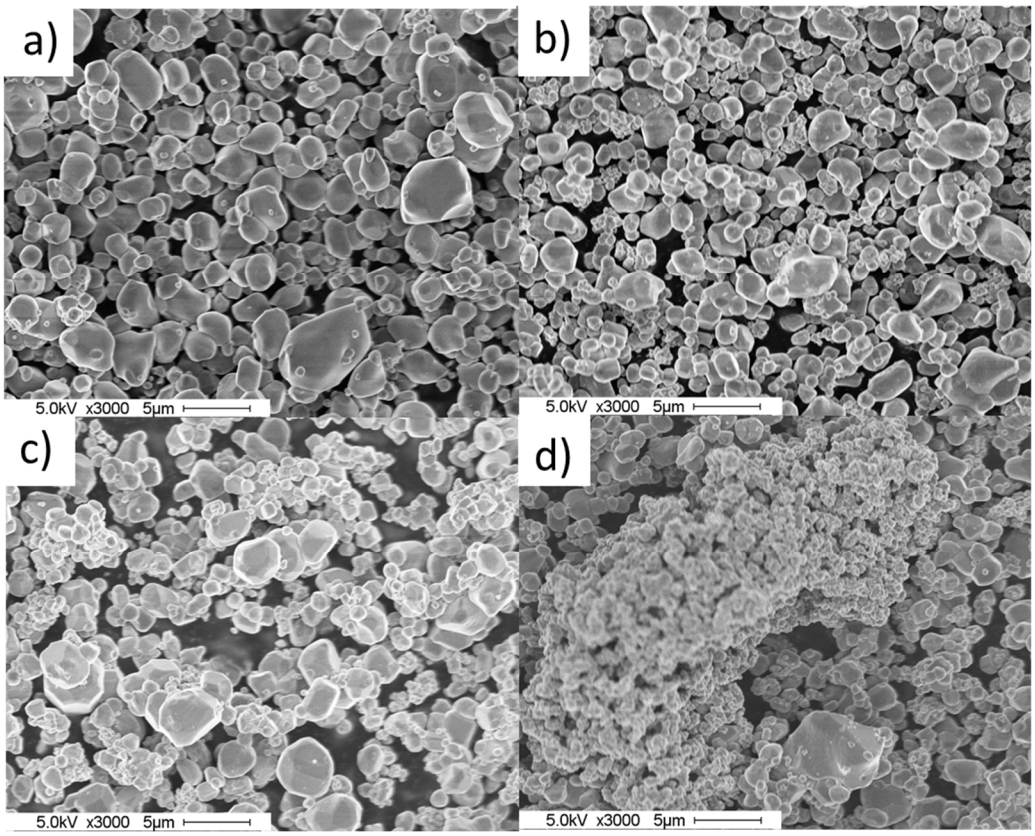

Fig. 4 SEM images of (a) the bare CTO sample, and the Pr(1.0,*z*)/CTO samples, where the *z* K was (b) 573, (c) 773 and (d) 1223.

Fig. 5 shows Ag K-edge XANES and XRD of the representative Ag-loaded samples. XANES spectra (Fig. 5A) show that the chemical states of Ag cocatalyst were metallic in all the Ag(3.5)/CTO and Ag(3.5)/Pr(1.0,*z*)/CTO (*z*=773 and 1223) samples. The diffraction from Ag metal was observed in the XRD patterns of all the Ag(3.5)/CTO and Ag(3.5)/Pr(1.0,*z*)/CTO (*z*=573, 773, 973, and 1223) samples (Fig. 5B). These results mean that the addition of Pr_6O_{11} did not influence the oxidation state of the deposited Ag NPs in these samples. The crystalline sizes of Ag NPs were calculated by the Scherrer equation using the diffraction line at $2\theta = 38.2°$ (Table S2). The average Ag particle size in the Ag(3.5)/CTO sample was 36.3 nm and that of the Ag(3.5)/Pr(1.0,*z*)/CTO samples was in the range of 46–55 nm. This means that the size of Ag NPs was slightly influenced by the Pr_6O_{11} species that was loaded in advance on the CTO particles.

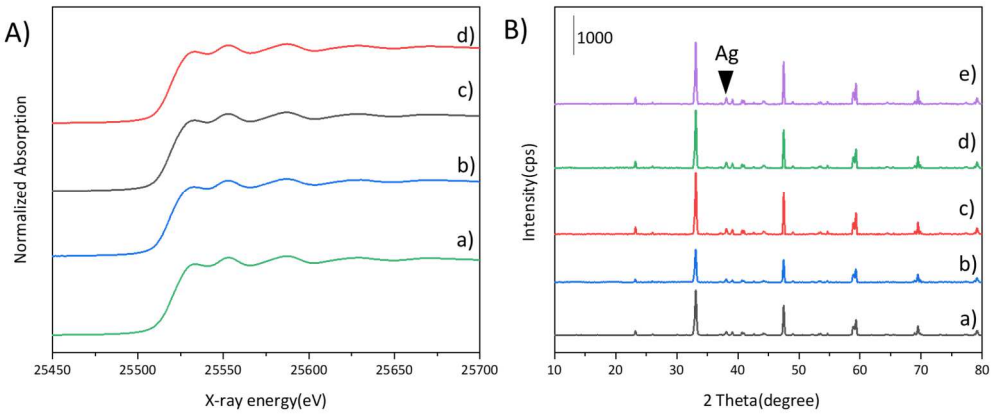

Fig. 5. [A] Ag K-edge EXANS of (a) Ag foil, (b) the Ag(3.5)/CTO sample and the Ag(3.5)/Pr(1.0,*z*)/CTO samples, where *z* K was (c) 773, and (d) 1223; **[B]** XRD spectra of (a) the Ag(3.5)/CTO sample and the Ag(3.5)/Pr(1.0, *z*)/CTO samples, where *z* K was (b) 573, (c) 773, (d) 973, and (e) 1223.

Fig. 6 displays the STEM-EDX analysis of the Ag(3.5)/Pr(1.0,773)/CTO sample. In the STEM image, a large CTO crystal and a semi-spherical Ag NP attached on the surface were observed (Fig. 6a), where the elemental assignments were confirmed by EDX mapping (Fig. 6b, d–f). Pr species existed not on the Ag NP but at the same place with the CTO particle. (Fig. 6c). The line analysis clarified that the presence of Ag NP on the surface (Fig. 6h) and the Pr species located between the CTO surface and Ag NP as a surface layer (Fig. 6i). In addition, the line analysis of oxygen elements had two peaks (Fig. 6g). The left peak position coincided with those for Ca and Ti (Fig. 6j–k), which indicates that the band is derived from CTO. On the other hand, the right peak (Fig. 6l) was more apparent than the shoulder peaks for Ca and Ti, and the position of this right peak showed a good agreement with the peak position for the Pr species (Fig. 6i). Considering that Pr_6O_{11} was confirmed on the XRD pattern of the Pr(1.0,773)/CTO sample (Fig. 1Bc), the observed right peak for oxygen would be partly derived from the Pr_6O_{11} species. Therefore, it is reasonable to conclude that the Pr_6O_{11} species were located as a thin layer between the CTO surface and the Ag NPs. The surface layers were also confirmed on the Pr(1.0,773)/CTO sample before loading Ag NPs (Fig. S4 and Fig. 1Bc). Thus, it is that the photodeposition produced the Ag NPs on the surface Pr_6O_{11} layers by the photodeposition, in other words, the photoexcited electrons exiting at the surface Pr_6O_{11} layers reduced Ag^+ cations in the aqueous solution, resulting the Ag NPs located on the surface Pr_6O_{11} layers covering the CTO particles.

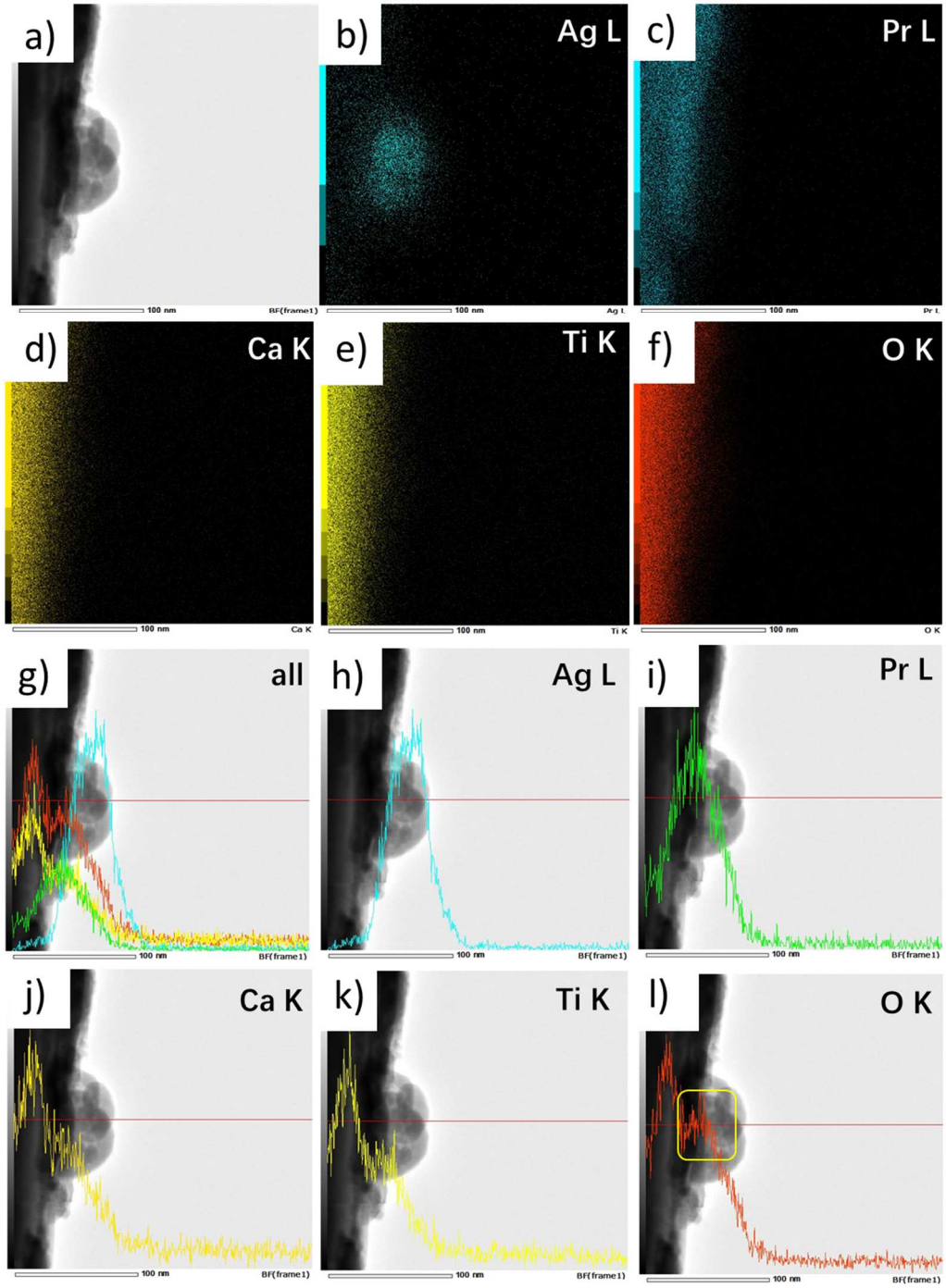

Fig. 6. STEM images, elemental mappings, and line analysis of the fresh Ag(3.5)/Pr(1.0,773)/CTO sample.

2.2. Photocatalytic activity tests of CO_2 reduction

Photocatalytic activity tests of CO_2 reduction by H_2O were carried out for various samples with or without Pr species that was prepared under the different calcination temperatures (Fig. 7). Compared with the non-modified CTO sample (Fig. 7a), the modification of Pr slightly decreased both the production rates of all the gases and the selectivity to CO (Fig. 7b). Similar to our previous

results,[28] loading of Ag NPs (3.5 wt%) into the CTO photocatalyst increased the formation of CO and O_2 drastically (Fig. 7c). The enhancement of the activity by adding Ag NPs would result from the cocatalyst property of the Ag NPs for CO formation, which provided the high CO selectivity such as 97.7%. Meanwhile, the blank experiments proved that photoirradiation and photocatalyst are both the indispensable conditions (Table S3), indicating that the present reactions are actual photocatalytic reactions.

The Ag(3.5)/Pr(1.0,573)/CTO sample (Fig. 7f) gave similar CO formation rate with both the Ag(3.5)/CTO sample and the Ag(3.5)/CTO(573) sample (Fig. 7c and d), meaning loading Pr species by the calcination at 573 K did not change the photocatalytic property. Contrary, the Ag(3.5)/Pr(1.0,773)/CTO sample provided enhanced activity by 1.4 times (Fig. 7g) without changing the high CO selectivity of 97.7 %, where the production rate of CO and O_2 were 32.3 and 12.6 μmol h^{-1}, respectively. Since the calcination at 773 K formed the Pr_6O_{11} layer between the CTO surface and the Ag NPs cocatalyst as mentioned above, the formation of this Pr_6O_{11} layer must contribute to this high photocatalytic production rate. The reason for the slightly lower O_2 production rate than the stoichiometric production rate will be discussed later. Separately, we confirmed that the optimal loading of Ag was 3.5 wt% in the Ag(*x*)/Pr(1.0,773)/CTO sample (Fig. S6). This optimum Ag loading was the same as our previous study on Ag/CTO photocatalysts.[28]

However, the high-temperature calcination of Pr-loaded CTO at 973 and 1223 K before loading Ag cocatalyst drastically decreased the photocatalytic activity of the Ag(3.5)/Pr(1.0,*z*)/CTO samples (Fig. 7h and i). As mentioned above, the calcination temperature (*z*) in Ag(3.5)/Pr(1.0,*z*)/CTO did not affect the particle size of the Ag NPs, suggesting that the presence and state of Pr influenced the photocatalytic activity in the Ag(3.5)/Pr(1.0,*z*)/CTO samples. As suggested by the SEM image of the Pr(1.0,1223)/CTO sample (Fig. 3d), the decrease of the photocatalytic activity would be related to the Pr doping into the CTO crystal and thus the decrease of the size of CTO particles. Judging from this, the doping might take place to some extent, also in the Pr(1.0,973)/CTO sample.

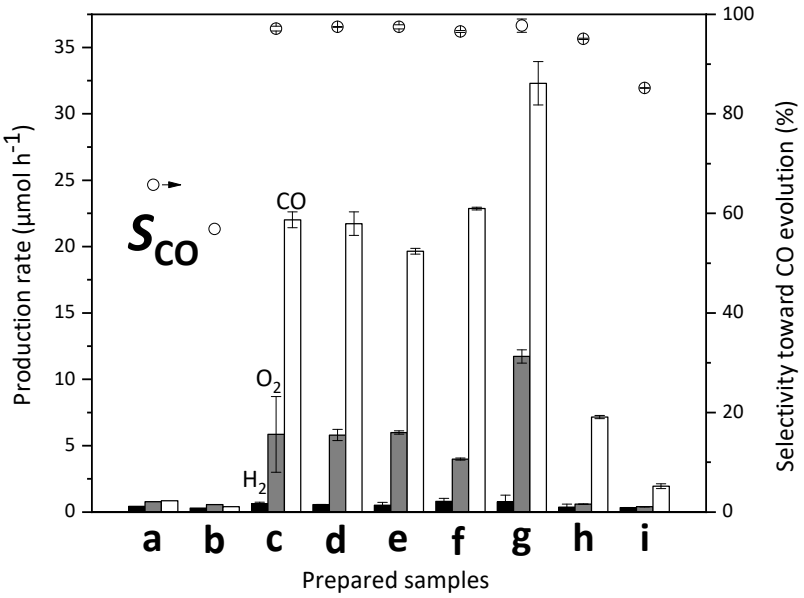

Fig. 7. Formation rates of H_2 (black), CO (white), and O_2 (gray), and the selectivity to CO (S_{CO}%, open circles) in the photocatalytic reaction tests for CO_2 reduction by H_2O with (a) the bare CTO sample, (b) the Pr(1.0,773)/CTO sample, (c) the Ag(3.5)/CTO sample, and the

Ag(3.5)/CTO(*z*) samples, where the *z* K was (d) 773 and (e) 1223, as well as the Ag(3.5)/Pr(1.0,*z*)/CTO samples, where the *z* K was (f) 573, (g) 773, (h) 973 and (i) 1223. The data were taken 3.5 h later from the start of photoirradiation.

The Ag(3.5)/Pr(*y*,773)/CTO samples consisting of various loading amount of the Pr species were examined for the photocatalytic reaction test (Fig. S7). There was a volcano-type relationship between the loading amount and the formation rates of CO and O_2, showing that the optimum amount was 1.0 wt%, while the selectivity to CO did not change drastically with all the Pr loading (S_{CO} > 96 %), indicating that a thin Pr_6O_{11} layer with poor crystallinity would facilitate the reaction. As shown in Fig. 7b, without loading Ag NPs, the Pr loading to the bare CTO sample had a negative effect on the photocatalytic activity, indicating that Pr_6O_{11} species would not solely contribute to the enhancement of the photocatalytic activity. The decrease in the photocatalytic activity at high Pr loading might be attributed to some reasons. One is that, since the Pr_6O_{11} species also absorbed the light of the UV region (λ < 350 nm, Fig. S1), the excess Pr_6O_{11} species may shade the UV light required for the excitation of the CTO photocatalyst. Another is that the excess Pr_6O_{11} species that had no interaction with the Ag NPs cocatalyst might change the surface property of the CTO photocatalyst to decrease the photocatalytic activity.

The stability test of the optimal Ag(3.5)/Pr(1.0,773)/CTO sample was performed (Fig. 8). Meanwhile, the resulting solution after the reaction test for 8 h was also analyzed by GC-MS (Fig. S8). Except for an internal standard decane peak at around 12 min, the rest are silica-related compounds leached from the column. It shows that in this reaction, no organic products possibly reduced from CO_2 such as alcohol or aldehydes were formed in the aqueous solution. In Fig. 8, the CO formation rate was stable for 8 h without marked deactivation. Contrary, the production rate of O_2 increased in the initial 3.5 h and then reached the steady-state. The O_2 evolution rate less than the stoichiometry of the products in CO_2 reduction (Eq. 1–3) in the initial period have been discussed so far, where some reasons have been proposed such as photoabsorption of O_2 on the photocatalyst surface and production of other oxidized compounds.[44] As another possibility, dissolution of O_2 in the aqueous solution in the initial stage should not be ignored especially in a large reactor containing 1.5 L of aqueous solution employed in the present study. After 2 h, the $R(e^-/h^+)$ value was near to 1.0, which indicates that the reaction proceeded in the chemically stoichiometric ratio in Eq. 1–3.

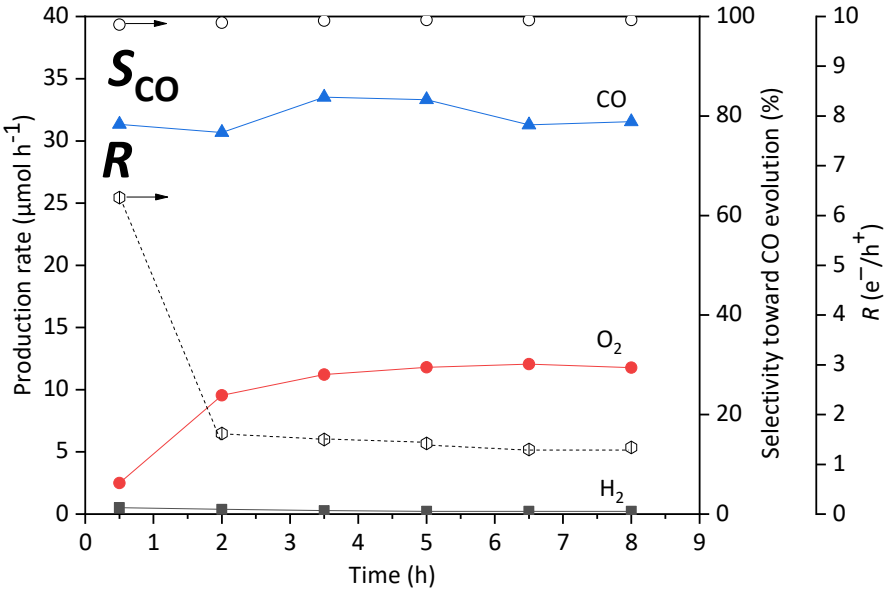

Fig. 8. Time course of CO (triangles), O_2 (closed circles), H_2 (squares), S_{CO} (open circles) and $R(e^-/h^+)$ (hexagon) in the photocatalytic reaction test for CO_2 reduction with water by using the Ag(3.5)/Pr(1.0,773)/CTO sample.

We analyzed the structure of the Ag(3.5)/Pr(1.0,773)/CTO sample after the reaction for 3.5 h by STEM-EDX, which revealed that there was no observable change in the structure of the sample although a part of the Pr species migrated on the Ag NPs (Fig. 9). These results demonstrated that the Ag(3.5)/Pr(1.0,773)/CTO sample has high stability under the reaction conditions of the photocatalytic CO_2 reduction and the Pr_6O_{11} layer and the migration of the Pr species evidenced the high affinity between the Pr_6O_{11} species and the Ag NPs, which suggested that this migration contributes to the stability of the Ag NPs cocatalyst. After the second use (Fig. S9), the experimental results did not change significantly, indicating that the observed movement of Pr species did not affect the photocatalytic activity for CO_2 reduction.

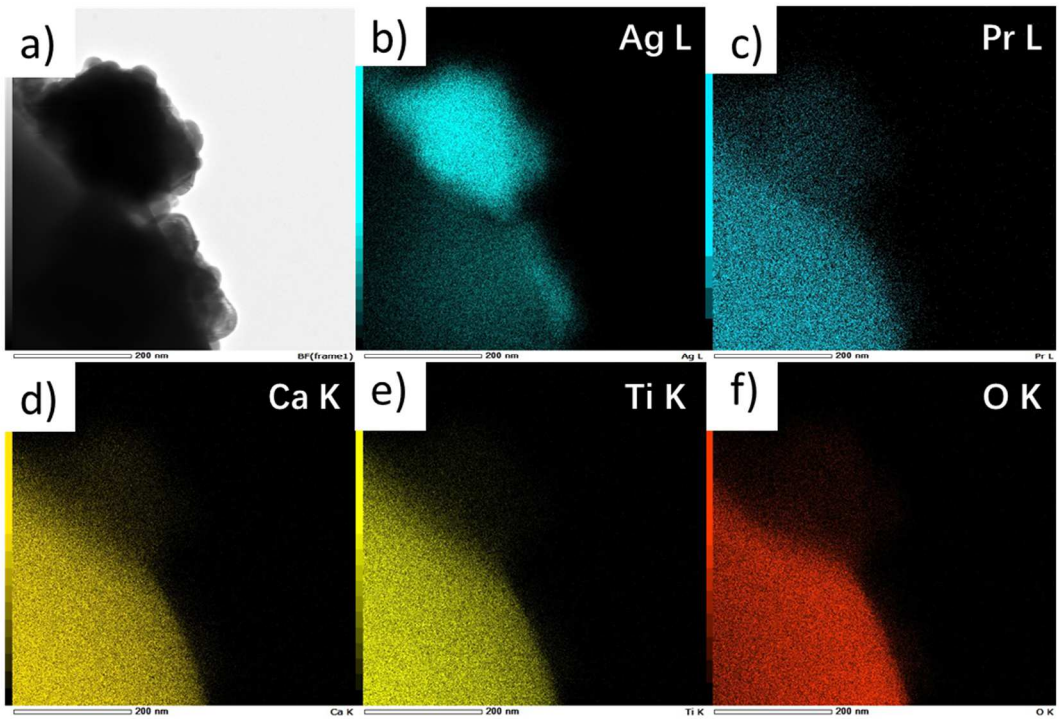

Fig. 9. STEM images, and elemental mappings of the used Ag(3.5)/Pr(1.0,773)/CTO sample for the photocatalytic reaction test.

2.3. Proposed mechanism

Fig. 10 shows the proposed enhancement mechanism of the photocatalytic activity by Pr_6O_{11} modification on the CTO photocatalyst with Ag cocatalyst. As is well known, the impregnation method would assist Pr_6O_{11} to cover indiscriminately all the surfaces of CTO. In other words, Pr_6O_{11} would cover both reduction facet and oxidation facet. In the reduction facet, the Pr_6O_{11} surface layer was found between the CTO surface and the Ag NPs. Since the energy level of the conduction band minimum of $CaTiO_3$ (− 0.8 eV)[1] is more negative than that of Pr_6O_{11} (− 0.64 eV),[21] it is energetically possible for the photoexcited electrons to transfer from the conduction band of the CTO particles to that of Pr_6O_{11} surface layer. Since the Pr_6O_{11} surface layer has both Pr(III) and Pr(IV) cations, it can easily accept the electrons tentatively.[23, 45] Recently, it was reported that a thin layer of CrO_x layer in well-known core–shell structured Rh/CrO_x cocatalyst can promote selective electron transfer from semiconductor photocatalyst to the Rh metal cocatalyst while suppress hole transfer,[46] which supports the above proposed electron transfer ability of the Pr_6O_{11} layer since both cations, Pr and Cr, have possible multiple valence states. On the other hand, the Pr_6O_{11} moiety located on the oxidative facet of CTO had no acceleration for O_2 evolution (Table S4), which indicates that Pr_6O_{11} layer has the same function as CrO_x layer selectively to boost the electron transfer selectively.

This electron-rich layer would provide electrons to the Ag NPs efficiently. Such electron migration would promote the special separation of the photoexcited electron-hole pairs to decrease the rapid recombination of the electrons and holes. Although the transport of holes is also possible, the deposition of Ag NPs during the photodeposition method suggests that the photoexcited electrons preferably to migrate to the Pr_6O_{11} surface layer and the holes mainly participate in the oxidation reaction on the CTO surface during both the photodeposition

procedure and the photocatalytic reaction. In addition, a part of the Pr species migrated to the Ag NPs, which might contribute to the high photocatalytic activity and stability.

On the other hand, Pr species can be doped into CTO lattice at the high calcination temperature such as 1223 K. Based on the previous report,[47] Pr^{3+} cation substituted the Ca^{2+} site of the $CaTiO_3$ lattices with the formation of a positive charge defect. Such a doped Pr^{3+} cation or defect is expected to have both positive effect and negative effect; it increases the carrier, and it might act as a recombination center for the photogenerated carriers. Another effect of doping was decrease of the size of the CTO particles, which decreases the photocatalytic activity for the photocatalytic CO_2 reduction with water.[28, 48] Thus, moderate calcination temperature at 773 K would be suitable for the formation of the Pr_6O_{11} phase on the surface of the CTO particle without doping of Pr^{3+} species into the CTO lattice, which contributed to the enhanced photocatalytic activity. An excess Pr_6O_{11} phase would form a thick surface layer, which may reduce the efficiency of the electron transfer or absorb the incident light of the wide wavelength from UV to visible light (Fig. S1).

According to the literature by Huang et al.[24], in the case of the Ag-loaded Pr-modified Ga_2O_3 ($Ag/Pr/Ga_2O_3$) photocatalysts, Pr(III) species were supported as hydroxide ($Pr(OH)_3$) and oxycarbonates ($Pr_2O_2CO_3$) before the photocatalytic reaction tests, and these Pr species were transformed to the Pr carbonate hydrates ($Pr_2(CO_3)_3{\cdot}8H_2O$) during the photocatalytic reaction for 5 h in an aqueous solution. The authors proposed that such Pr species accumulated and decomposed CO_2 over the Ga_2O_3 photocatalyst with an Ag cocatalyst. On the other hand, in the present Pr(1.0,773)/CTO and Pr(10.0,773)/CTO samples, the Pr species was assigned to Pr_6O_{11} phase (Fig. 1) and there were no diffraction peaks assignable to other Pr species such as $Pr_2O_2CO_3$ and $Pr_2(CO_3)_3{\cdot}8H_2O$ even when Pr(*y*,773)/CTO samples were dried after soaking in the 1.0 M $NaHCO_3$ aqueous solution for 5 h with the flow of CO_2 in the same manner as the reaction tests (Fig. S10b–c). But in Fig. S10a, the wet Pr(1.0,773)/CTO sample with the solution showed a very small broad peak around 27.5 ° possibly assignable to $Pr(OH)_3$[49] in addition to the almost unchanged diffraction from Pr_6O_{11}, while there is no $Pr_2O_2CO_3$ peak (26.3 °).[50] This diffraction at 27.5 ° disappeared when dried as mentioned (Fig. S10b). It is clarified that $Pr(OH)_3$ was unstable on the CTO surface. It is suggested that during the photocatalytic reaction test the predominant Pr species would be in the Pr_6O_{11} form, which should be originated from the property of the $CaTiO_3$. However, it cannot be completely excluded that the possibly formed $Pr(OH)_3$ species may contribute to the CO_2 adsorption to promote the photocatalytic CO_2 reduction as proposed. Among the praseodymium oxides (Pr_2O_3, Pr_7O_{12}, and Pr_6O_{11}), the Pr_6O_{11} phase was the most stable,[51] and the hexagonal Pr_2O_3 phase could partly transform to the hexagonal $Pr(OH)_3$ in the aqueous solution. Anyway, the major Pr_6O_{11} surface layer is proposed to give a positive effect on the photocatalytic activity.

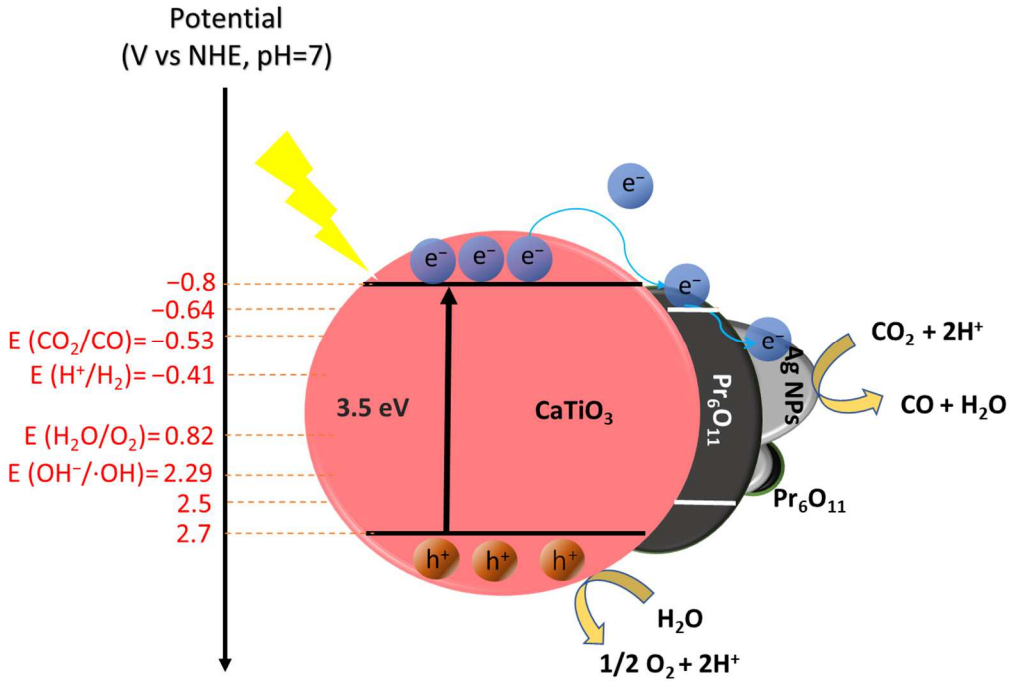

Fig. 10. Schematic diagram of CO_2 reduction with H_2O in the Ag(3.5)/Pr(1.0,773)/CTO photocatalyst.

Conclusion

We demonstrated that the loading of Pr_6O_{11} on the surface of $CaTiO_3$ enhanced the activity of Ag-modified $CaTiO_3$ photocatalyst for the photocatalytic CO_2 reduction with H_2O as an electron donor. The optimal sample showed high production rate of CO (32.3 μmol h^{-1}), which was enhanced by 1.4 times by the Pr_6O_{11} modification, with keeping high the selectivity to CO (97.7 %) and high stability of photocatalytic performance for the long-time reaction without changing the structure. Moreover, it was revealed that the moderate loading and calcination temperature at 773 K was vital to obtain the enhanced activity, where Pr_6O_{11} existed as a surface thin layer located between the $CaTiO_3$ surface and the Ag NPs cocatalyst. It was confirmed that the Pr_6O_{11} species did not enhance the oxidative activity by photoformed holes. Thus, we proposed that the enhanced activity was obtained by the efficient and selective electron transfer from the CTO particles to Ag NPs through the Pr_6O_{11} layer. Unlike the Pr species such as $Pr(OH)_3$ and $Pr_2(CO_3)_3{\cdot}8H_2O$ formed on the different photocatalysts reported in the literature,[24] the property and stability of Pr_6O_{11} in water were also the essential factors to improve the photocatalytic reaction. We believed that this approach is applicable to enhance the photocatalytic activity for CO_2 reduction and contributes to developing novel photocatalytic composite materials.

■ ASSOCIATED CONTENT

Supporting Information

DR UV-vis spectra of a pure Pr_6O_{11}; the calculation for the particle sizes of $CaTiO_3$ in various samples; SSA of the bare CTO(*z*) and Pr(1.0,*z*)/CTO samples; the additional morphologies and elemental analysis by SEM, STEM and SEM-EDS; properties about Ag NPs of prepared samples; the optimal loading for Pr and Ag; the XRD patterns for the samples dispersed in $NaHCO_3$ solution with the flow

of CO_2.

■ AUTHOR INFORMATION

Author contributions

Hongxuan Qiu: Conceptualization, Investigation, Writing original draft. Akihiko Anzai: Investigation. Tayyebeh Soltani: Investigation. Akira Yamamoto: Investigation, Funding acquisition. Eri Fudo: Investigation. Atsuhiro Tanaka: Investigation. Hiroshi Kominami: Investigation. Hisao Yoshida: Conceptualization, Supervision, Reviewing and Editing manuscript, Funding acquisition.

Notes

The authors declare no competing financial interest.

■ Acknowledgements

The XAFS measurements were performed at the BL01B1 of SPring-8 with the approval of the Japan Synchrotron Radiation Research Institute (JASRI) (Proposal no. 2020A1316). This work was financially supported by ISHIZUE 2020 of the Kyoto University Research Development Program, and a Grant-in-Aid for Challenging Research (Exploratory, 20K21108) from the Japan Society for the Promotion of Science (JSPS), and the Program for Element Strategy Initiative for Catalysts & Batteries (ESICB, JPMXP0112101003), commissioned by the MEXT of Japan. HQ appreciates the China Scholarship Council providing a scholarship (CSC.202006260014).

■ References

1. Soltani, T.; Yamamoto, A.; Singh, S. P.; Anzai, A.; Fudo, E.; Tanaka, A.; Kominami, H.; Yoshida, H., Simultaneous Formation of CO and H_2O_2 from CO_2 and H_2O with a Ag–MnO_x/$CaTiO_3$ Photocatalyst. *ACS Applied Energy Materials* **2021,** *4* (7), 6500-6510.

2. Bagger, A.; Christensen, O.; Ivaništšev, V.; Rossmeisl, J., Catalytic CO_2/CO Reduction: Gas, Aqueous, and Aprotic Phases. *ACS Catalysis* **2022,** *12* (4), 2561-2568.

3. Chu, S.; Cui, Y.; Liu, N., The path towards sustainable energy. *Nature Materials* **2017,** *16* (1), 16-22.

4. Shafaat, H. S.; Yang, J. Y., Uniting biological and chemical strategies for selective CO_2 reduction. *Nature Catalysis* **2021,** *4* (11), 928-933.

5. Huang, H.; Shi, R.; Li, Z.; Zhao, J.; Su, C.; Zhang, T., Triphase Photocatalytic CO_2 Reduction over Silver-Decorated Titanium Oxide at a Gas–Water Boundary. *Angewandte Chemie International Edition* **2022,** *61* (17), e202200802.

6. Wang, K.; Du, Y.; Li, Y.; Wu, X.; Hu, H.; Wang, G.; Xiao, Y.; Chou, S.; Zhang, G., Atomic-level insight of sulfidation-engineered Aurivillius-related $Bi_2O_2SiO_3$ nanosheets enabling visible light low-concentration CO_2 conversion. *Carbon Energy* **2023,** *5* (2), e264.

7. Xiong, X.; Mao, C.; Yang, Z.; Zhang, Q.; Waterhouse, G. I. N.; Gu, L.; Zhang, T., Photocatalytic CO_2 Reduction to CO over Ni Single Atoms Supported on Defect-Rich Zirconia. *Advanced Energy Materials* **2020,** *10* (46), 2002928.

8. Zhang, J.; Haribal, V.; Li, F., Perovskite nanocomposites as effective CO_2-splitting agents in a cyclic redox scheme. *Science Advances* **2017,** *3* (8), e1701184.

9. Wang, Y.; Zhang, C.; Li, R., Modulating the Selectivity of Photocatalytic CO_2 Reduction in Barium Titanate by Introducing Oxygen Vacancies. *Transactions of Tianjin University* **2022,** *28* (4), 227-235.

10. Wang, S.; Teramura, K.; Hisatomi, T.; Domen, K.; Asakura, H.; Hosokawa, S.; Tanaka, T., Optimized Synthesis of Ag-Modified Al-Doped $SrTiO_3$ Photocatalyst for the Conversion of CO_2 Using H_2O as an Electron Donor. *ChemistrySelect* **2020,** *5* (28), 8779-8786.

11. Iizuka, K.; Wato, T.; Miseki, Y.; Saito, K.; Kudo, A., Photocatalytic Reduction of Carbon Dioxide over Ag Cocatalyst-Loaded $ALa_4Ti_4O_{15}$ (A = Ca, Sr, and Ba) Using Water as a Reducing Reagent. *Journal of the American Chemical Society* **2011,** *133* (51), 20863-20868.

12. Yamamoto, M.; Yoshida, T.; Yamamoto, N.; Nomoto, T.; Yamamoto, Y.; Yagi, S.; Yoshida, H., Photocatalytic reduction of CO_2 with water promoted by Ag clusters in Ag/Ga_2O_3 photocatalysts. *Journal of Materials Chemistry A* **2015,** *3* (32), 16810-16816.

13. Pang, R.; Teramura, K.; Asakura, H.; Hosokawa, S.; Tanaka, T., Highly selective photocatalytic conversion of CO_2 by water over Ag-loaded $SrNb_2O_6$ nanorods. *Applied Catalysis B: Environmental* **2017,** *218*, 770-778.

14. Li, W.; Yu, R.; Li, M.; Guo, N.; Yu, H.; Yu, Y., Photocatalytical degradation of diclofenac by Ag-BiOI-rGO: Kinetics, mechanisms and pathways. *Chemosphere* **2019,** *218*, 966-973.

15. Singh, J.; Soni, R. K., Efficient charge separation in Ag nanoparticles functionalized ZnO nanoflakes/CuO nanoflowers hybrids for improved photocatalytic and SERS activity. *Colloids and Surfaces A: Physicochemical and Engineering Aspects* **2021,** *626*, 127005.

16. Kuila, A.; Saravanan, P.; Bahnemann, D.; Wang, C., Novel Ag decorated, BiOCl surface doped $AgVO_3$ nanobelt ternary composite with Z-scheme homojunction-heterojunction interface for high prolific photo switching, quantum efficiency and hole mediated photocatalysis. *Applied Catalysis B: Environmental* **2021,** *293*, 120224.

17. Ham, Y.; Hisatomi, T.; Goto, Y.; Moriya, Y.; Sakata, Y.; Yamakata, A.; Kubota, J.; Domen, K., Flux-mediated doping of $SrTiO_3$ photocatalysts for efficient overall water splitting. *Journal of Materials Chemistry A* **2016,** *4* (8), 3027-3033.

18. Pomiro, F. J.; Gaviría, J. P.; Fouga, G. G.; Vega, L. D.; Bohé, A. E., Chlorination of Pr_2O_3 and Pr_6O_{11}. Crystal structure, magnetic and spectroscopic properties of praseodymium oxychloride. *Journal of Alloys and Compounds* **2019,** *776*, 919-926.

19. Taguchi, H.; Chiba, R.; Komatsu, T.; Orui, H.; Watanabe, K.; Hayashi, K., LNF SOFC cathodes with active layer using Pr_6O_{11} or Pr-doped CeO_2. *Journal of Power Sources* **2013,** *241*, 768-775.

20. Zhang, P.; Niu, T.; Zheng, G.; Liu, L.; Deng, J.; Jin, Y.; Jiao, Z.; Sun, X., Synthesis and characterization of Pr_6O_{11} and Ag/Pr_6O_{11} nanorods and their photocatalytic activity toward dye degradation. *Materials Letters* **2017,** *203*, 54-57.

21. Shende, A. G.; Ghugal, S. G.; Vidyasagar, D.; Kokane, S. B.; Jagannath; Umare, S. S.; Sasikala, R., Solvent free solid-state synthesis of $Pr_6O_{11}/g\text{-}C_3N_4$ visible light active photocatalyst for degradation of AV7 dye. *Materials Research Bulletin* **2018,** *107*, 154-163.

22. Balachandran, S.; Thirumalai, K.; Swaminathan, M., Facile hydrothermal synthesis of a highly efficient solar active Pr_6O_{11}–ZnO photocatalyst and its multiple applications. *RSC Advances* **2014,** *4* (53), 27642-27653.

23. Kim, J.-S.; Na, C. W.; Kwak, C.-H.; Li, H.-Y.; Yoon, J. W.; Kim, J.-H.; Jeong, S.-Y.; Lee, J.-H., Humidity-Independent Gas Sensors Using Pr-Doped In_2O_3 Macroporous Spheres: Role of Cyclic Pr^{3+}/Pr^{4+} Redox Reactions in Suppression of Water-Poisoning Effect. *ACS Applied Materials & Interfaces* **2019,** *11* (28), 25322-25329.

24. Huang, Z.; Teramura, K.; Asakura, H.; Hosokawa, S.; Tanaka, T., CO_2 capture, storage, and conversion using a praseodymium-modified Ga_2O_3 photocatalyst. *Journal of Materials Chemistry A* **2017,** *5* (36),

19351-19357.
25. Shimura, K.; Kawai, H.; Yoshida, T.; Yoshida, H., Bifunctional Rhodium Cocatalysts for Photocatalytic Steam Reforming of Methane over Alkaline Titanate. *ACS Catalysis* **2012,** *2* (10), 2126-2134.
26. Zhu, X.; Yamamoto, A.; Imai, S.; Tanaka, A.; Kominami, H.; Yoshida, H., Facet-selective deposition of a silver–manganese dual cocatalyst on potassium hexatitanate photocatalyst for highly selective reduction of carbon dioxide by water. *Applied Catalysis B: Environmental* **2020,** *274*, 119085.
27. Yoshida, H.; Zhang, L.; Sato, M.; Morikawa, T.; Kajino, T.; Sekito, T.; Matsumoto, S.; Hirata, H., Calcium titanate photocatalyst prepared by a flux method for reduction of carbon dioxide with water. *Catalysis Today* **2015,** *251*, 132-139.
28. Anzai, A.; Fukuo, N.; Yamamoto, A.; Yoshida, H., Highly selective photocatalytic reduction of carbon dioxide with water over silver-loaded calcium titanate. *Catalysis Communications* **2017,** *100*, 134-138.
29. Naniwa, S.; Hishitani, S.; Yamamoto, A.; Yoshida, H., Ligand-to-metal charge transfer of a pyridine surface complex on TiO_2 for selective dehydrogenative cross-coupling with benzene. *Physical Chemistry Chemical Physics* **2021,** *23* (19), 11366-11373.
30. Ishii, T.; Anzai, A.; Yamamoto, A.; Yoshida, H., Calcium zirconate photocatalyst and silver cocatalyst for reduction of carbon dioxide with water. *Applied Catalysis B: Environmental* **2020,** *277*, 119192.
31. Anzai, A.; Fukuo, N.; Yamamoto, A.; Yoshida, H., Highly selective photocatalytic reduction of carbon dioxide with water over silver-loaded calcium titanate. *Catal. Commun.* **2017,** *100*, 134–138.
32. Peng, S.; Wang, Y.; Wang, H.; Dong, X.; Dong, L.; Gan, Y., Microstructure and Electrical Properties in Low- Sb_2O_3-Doped Pr_6O_{11} Ceramics. *Journal of the American Ceramic Society* **2012,** *95* (9), 2914-2918.
33. Abu-Zied, B. M., Controlled synthesis of praseodymium oxide nanoparticles obtained by combustion route: Effect of calcination temperature and fuel to oxidizer ratio. *Applied Surface Science* **2019,** *471*, 246-255.
34. Anzai, A.; Fujiwara, K.; Yamamoto, A.; Yoshida, H., Platinum-loaded lanthanum-doped calcium titanate photocatalysts prepared by a flux method for photocatalytic steam reforming of methane. *Catalysis Today* **2020,** *352*, 1-9.
35. Al Kutubi, H.; Rassaei, L.; Olthuis, W.; Nelson, G. W.; Foord, J. S.; Holdway, P.; Carta, M.; Malpass-Evans, R.; McKeown, N. B.; Tsang, S. C.; Castaing, R.; Forder, T. R.; Jones, M. D.; He, D.; Marken, F., Polymers of intrinsic microporosity as high temperature templates for the formation of nanofibrous oxides. *RSC Advances* **2015,** *5* (89), 73323-73326.
36. Gao, W.; Zhang, W.; Tian, B.; Zhen, W.; Wu, Y.; Zhang, X.; Lu, G., Visible light driven water splitting over $CaTiO_3/Pr^{3+}$-Y_2SiO_5/RGO catalyst in reactor equipped artificial gill. *Applied Catalysis B: Environmental* **2018,** *224*, 553-562.
37. Su, L.; Zhang, Y.; Zhan, X.; Zhang, L.; Zhao, Y.; Zhu, X.; Wu, H.; Chen, H.; Shen, C.; Wang, L., Pr_6O_{11}: Temperature-Dependent Oxygen Vacancy Regulation and Catalytic Performance for Lithium–Oxygen Batteries. *ACS Applied Materials & Interfaces* **2022,** *14* (36), 40975-40984.
38. Kumar, A.; Kumar, M.; Navakoteswara Rao, V.; Shankar, M. V.; Bhattacharya, S.; Krishnan, V., Unraveling the structural and morphological stability of oxygen vacancy engineered leaf-templated $CaTiO_3$ towards photocatalytic H_2 evolution and N_2 fixation reactions. *Journal of Materials Chemistry A* **2021,** *9* (31), 17006-17018.
39. Tian, X.; Wang, C.; Wen, J.; Lian, S.; Ji, C.; Huang, Z.; Chen, Z.; Peng, H.; Wang, S.; Li, J.; Hu, J.; Peng, Y., High temperature sensitivity phosphor based on an old material: Red emitting H_3BO_3 flux assisted $CaTiO_3$: Pr^{3+}. *Journal of Luminescence* **2019,** *214*, 116528.
40. Wang, S.; Shi, L.; Boubeche, M.; Wang, X.; Zeng, L.; Wang, H.; Xie, Z.; Tan, W.; Luo, H., Influence of

Ln elements (Ln = La, Pr, Nd, Sm) on the structure and oxygen permeability of Ca-containing dual-phase membranes. *Separation and Purification Technology* **2020,** *251*, 117361.

41. Kyômen, T.; Hanaya, M.; Takashima, H., Electroluminescence near interfaces between (Ca,Sr)TiO_3:Pr phosphor and SnO_2:Sb transparent conductor thin films prepared by sol–gel and spin-coating methods. *Journal of Luminescence* **2014,** *149*, 133-137.

42. Yan, X.; Li, S.; Bao, J.; Zhang, N.; Fan, B.; Li, R.; Liu, X.; Pan, Y.-X., Immobilization of Highly Dispersed Ag Nanoparticles on Carbon Nanotubes Using Electron-Assisted Reduction for Antibacterial Performance. *ACS Applied Materials & Interfaces* **2016,** *8* (27), 17060-17067.

43. Kudo, A.; Kato, H., Effect of lanthanide-doping into $NaTaO_3$ photocatalysts for efficient water splitting. *Chemical Physics Letters* **2000,** *331* (5), 373-377.

44. Zhu, X.; Anzai, A.; Yamamoto, A.; Yoshida, H., Silver-loaded sodium titanate photocatalysts for selective reduction of carbon dioxide to carbon monoxide with water. *Applied Catalysis B: Environmental* **2019,** *243*, 47-56.

45. Dubey, P. K.; Hong, J.; Anisur, M. R.; Lee, K.; Belko, S.; Singh, P., Enhanced Electrocatalytic Activity and Surface Exsolution in PrO_x-Substituted Cerium Gadolinium Oxide. *ACS Applied Energy Materials* **2023,** *6* (2), 657-666.

46. Kotani, T.; Ogawa, K.; Suzuki, H.; Kato, K.; Tomita, O.; Yamakata, A.; Abe, R., An unexplored role of the CrO_x shell in an elaborated Rh/CrO_x core–shell cocatalyst for photocatalytic water splitting: a selective electron transport pathway from semiconductors to core metals, boosting charge separation and H_2 evolution. *EES Catalysis* **2023**.

47. Wanjun, T.; Kun, W.; Xuhui, B.; Donghua, C., Synthesis of $CaTiO_3$:Pr,Al phosphors by a peroxide-based route and their photoluminescence properties. *Journal of Materials Science* **2007,** *42* (24), 9915-9919.

48. Yoshida, H.; Takeuchi, M.; Sato, M.; Zhang, L.; Teshima, T.; Chaskar, M. G., Potassium hexatitanate photocatalysts prepared by a flux method for water splitting. *Catalysis Today* **2014,** *232*, 158-164.

49. Zhai, T.; Xie, S.; Lu, X.; Xiang, L.; Yu, M.; Li, W.; Liang, C.; Mo, C.; Zeng, F.; Luan, T.; Tong, Y., Porous $Pr(OH)_3$ Nanostructures as High-Efficiency Adsorbents for Dye Removal. *Langmuir* **2012,** *28* (30), 11078-11085.

50. Sadhu, A.; Singh, S. P.; Bhattacharyya, S., Direct Correlation of the Morphologies of Metal Carbonates, Oxycarbonates, and Oxides Synthesized by Dry Autoclaving to the Intrinsic Properties of the Metals. *Crystal Growth & Design* **2014,** *14* (8), 4060-4067.

51. Abrutis, A.; Lukosius, M.; Saltyte, Z.; Galvelis, R.; Baumann, P. K.; Schumacher, M.; Lindner, J., Chemical vapour deposition of praseodymium oxide films on silicon: influence of temperature and oxygen pressure. *Thin Solid Films* **2008,** *516* (15), 4758-4764.

Supplementary data

Praseodymium oxide improving the activity of silver loaded calcium titanate photocatalyst for carbon dioxide reduction with water

Hongxuan Qiu,[a] Akihiko Anzai,[a] Tayyebeh Soltani,[a] Akira Yamamoto,[a,b] Eri Fudo,[c] Atsuhiro Tanaka,[d,e] Hiroshi Kominami,[d] and Hisao Yoshida[a,b*]

[a] *Kyoto University, Graduate School of Human and Environmental Studies, Kyoto 606-8501, Japan*

[b] *Kyoto University, Elements Strategy Initiative for Catalysts and Batteries (ESICB), Kyoto 615-8520, Japan*

[c] *Molecular and Material Engineering, Interdisciplinary Graduate School of Science and Engineering, Kindai University, 3-4-1 Kowakae, Higashiosaka, Osaka 577-8502, Japan.*

[d] *Department of Applied Chemistry, Faculty of Science and Engineering, Kindai University, 3-4-1 Kowakae, Higashiosaka, Osaka 577-8502, Japan*

[e] *Precursory Research for Embryonic Science and Technology (PRESTO), Japan Science and Technology Agency (JST), 4-1-8 Honcho, Kawaguchi 332-0012, Japan*

* yoshida.hisao.2a@kyoto-u.ac.jp

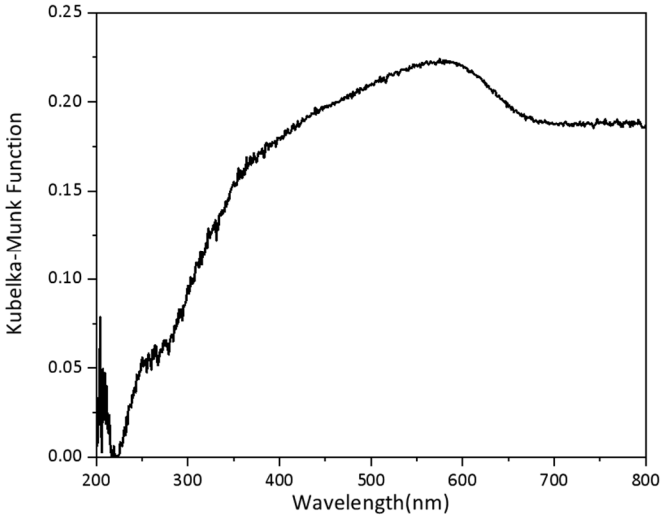

Fig. S1. DR UV-vis spectra of a pure Pr_6O_{11} sample diluted with $BaSO_4$ by a factor of 100 times in weight.

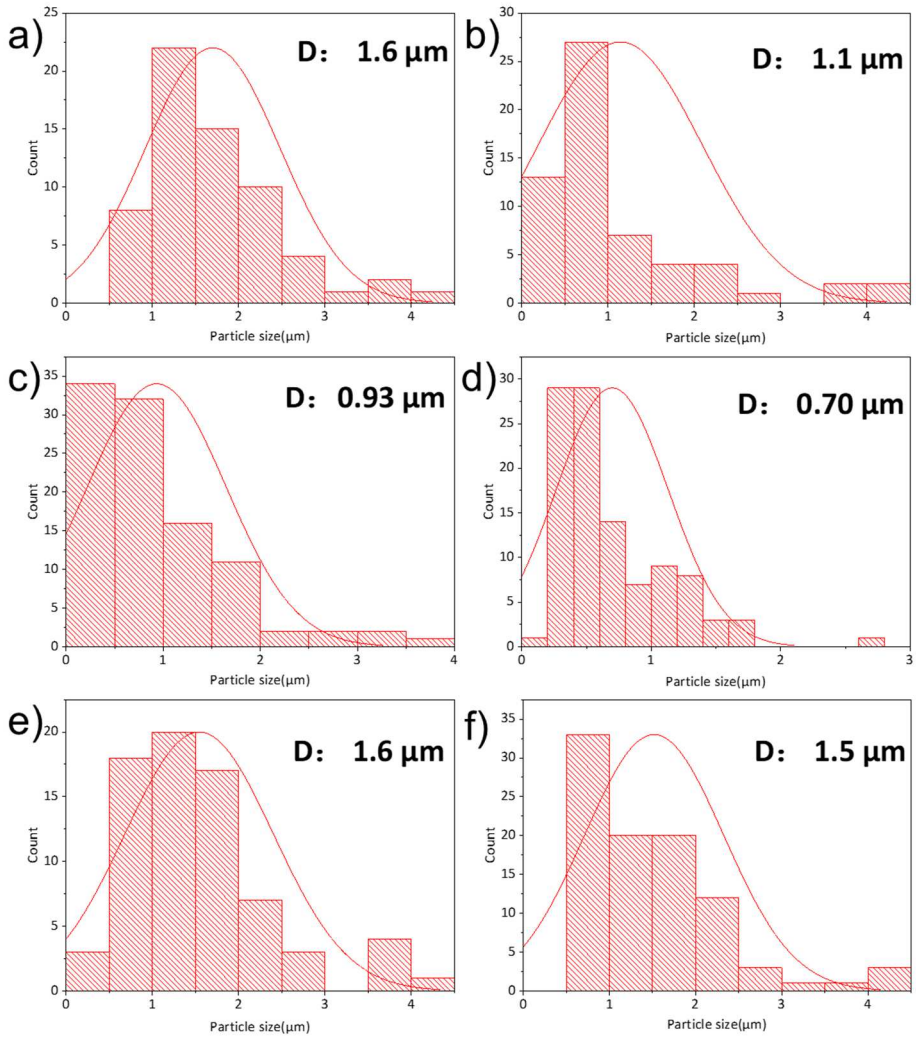

Fig. S2. The CTO particle size estimated from the SEM images of the samples in Fig. 3, (a) the bare CTO and the Pr(1.0,*z*)/CTO samples, where the *z* K was (b) 573, (c) 773, (d) 1223; and in Fig. S5e–f, (e) the bare CTO(573), and (f) the bare CTO(1223).

Table S1 SSA of the bare CTO(*z*) and Pr(1.0,*z*)/CTO samples

Entry	Sample	Specific surface area[a] / $m^2\ g^{-1}$
1	Bare CTO	2.0
2	Bare CTO(773)	2.0
3	Bare CTO(1223)	2.0
4	Pr(1.0,573)/CTO	2.4
5	Pr(1.0,773)/CTO	2.4
6	Pr(1.0,973)/CTO	2.2
7	Pr(1.0,1223)/CTO	2.3

[a] Estimated by a BET method from N_2 adsorption experiment at 77 K.

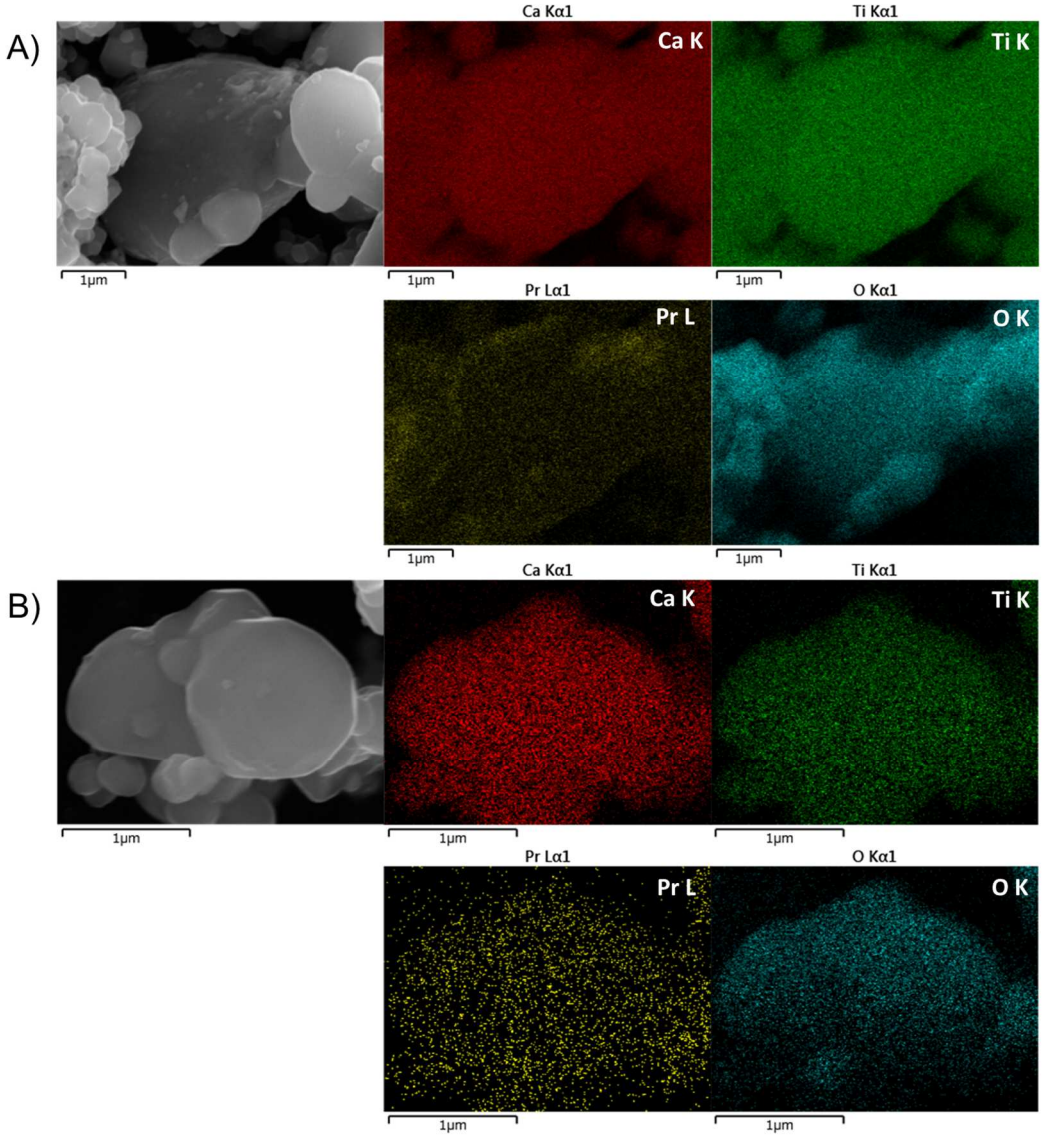

Fig. S3. SEM-EDS elemental images of **[A]** the Pr(1.0,773)/CTO sample, and **[B]** the Pr(1.0,1223)/CTO sample.

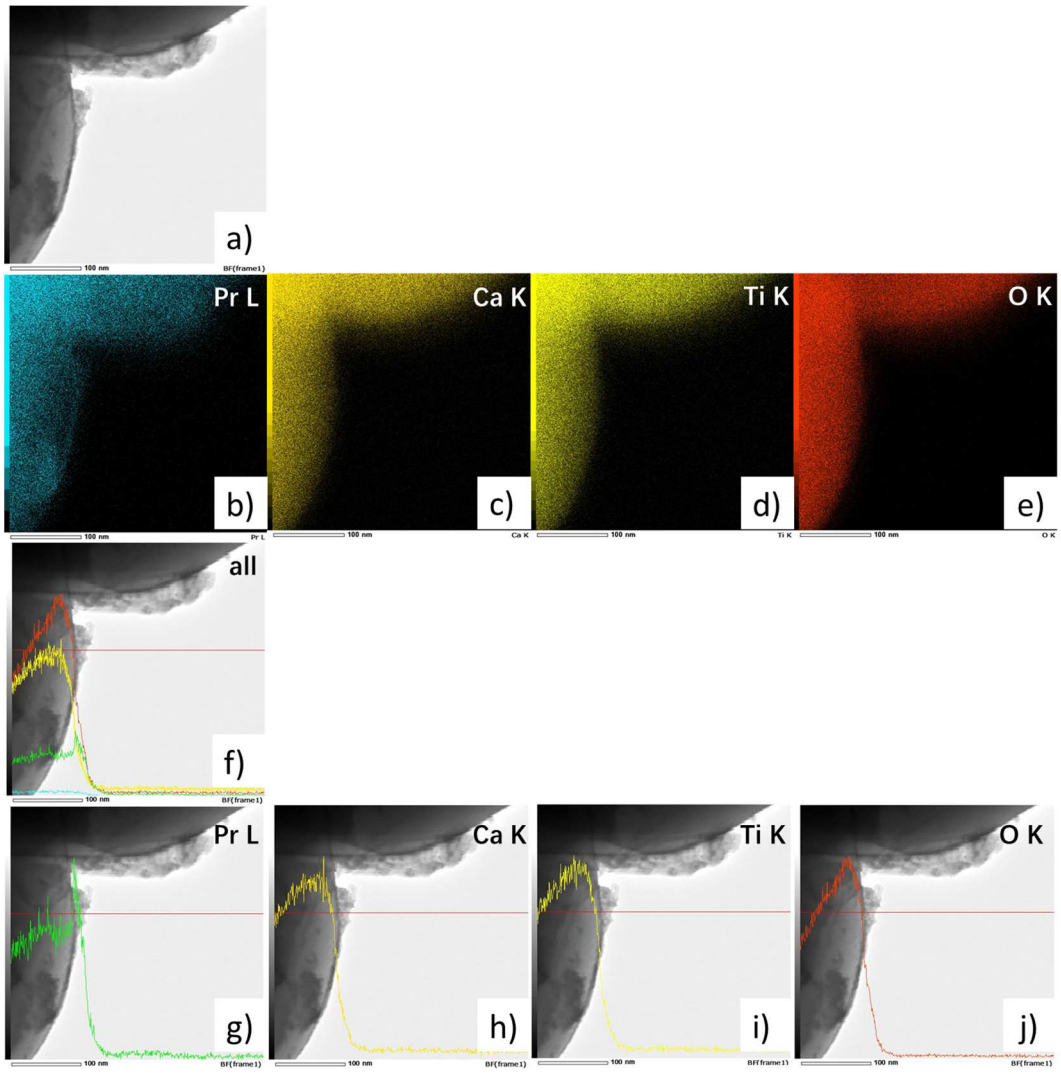

Fig. S4. STEM images, elemental mappings, and line analysis of the Pr(1.0,773)/CTO sample.

Fig. S4 shows the STEM images, elemental mappings, and line analysis of the Pr(1.0,773)/CTO sample. The mappings clarified that the Pr species existed on the CTO surface entirely (Fig. S4a–e). In the line analysis, the peak for the Pr signal at the edge of the CTO crystal clearly evidenced the presence of the Pr species on the surface (Fig. S4g).

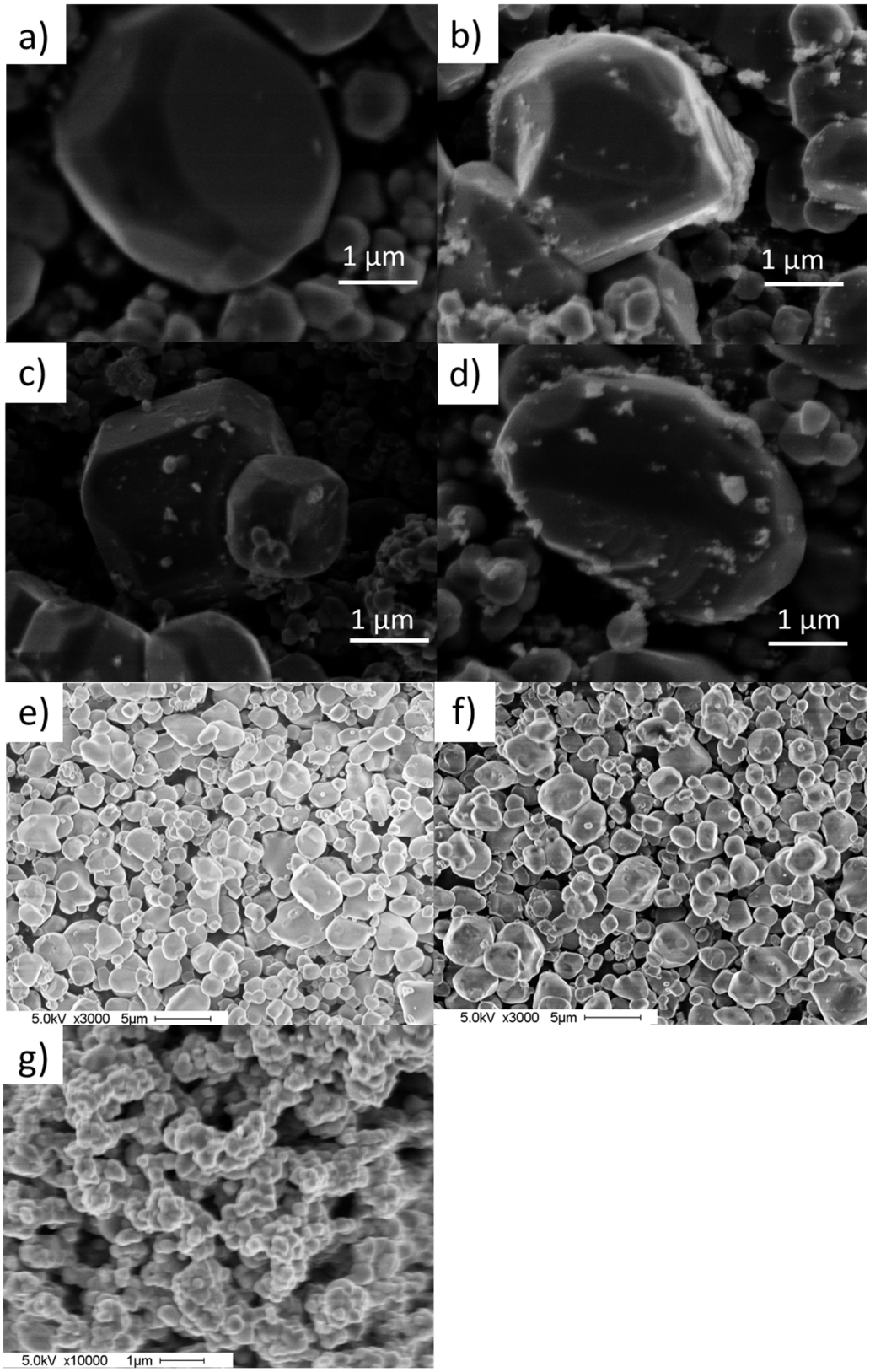

Fig. S5. SEM images of the samples, (a) bare CTO, (b) Ag(3.5)/CTO, (c) Pr(1.0,773)/CTO, (d) Ag(3.5)/Pr(1.0,773)/CTO, (e) bare CTO(573), (f) bare CTO(1223), and (g) Pr(1.0,1223)/CTO.

Table S2 Properties about Ag NPs of prepared samples.

Entry	Sample	Crystallites size (XRD) of Ag [a]/ nm	Loading amount of Ag [b]/ wt%
1	Ag(3.5)/CTO	36.3	3.48
2	Ag(3.5)/Pr(1.0,573)/CTO	46.4	3.48
3	Ag(3.5)/Pr(1.0,773)/CTO	50.2	3.49
4	Ag(3.5)/Pr(1.0,973)/CTO	54.2	3.46
5	Ag(3.5)/Pr(1.0,1223)/CTO	55.0	3.43

[a] Estimated by XRD patterns calculated from a line width at 2θ = 38.2°.

[b] Estimated by XRF measurements.

Table S3 Results of blank experiments for the reaction test with the Ag(3.5)/Pr(1.0,773)/CTO sample.

Entry	Condition	Production rate (μmol h^{-1}) [a]			S_{CO}(%)
		H_2	O_2	CO	
1	Without irradiation	0.0	0.0	0.0	0.0
2	Without photocatalyst	0.4	0.1	0.1	22.2

[a] The production rates were measured after 3.5 h of photoirradiation.

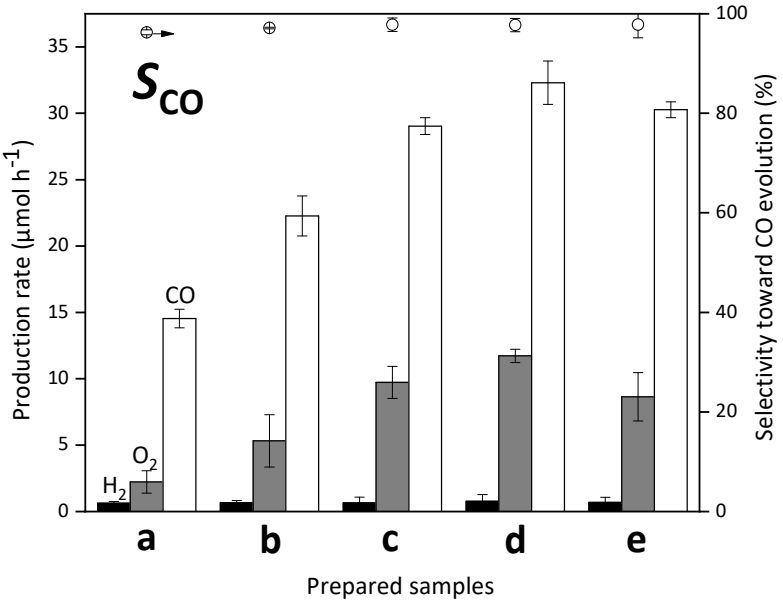

Fig. S6. Formation rates of the photocatalytic activity tests for CO_2 reduction, CO (white bar), H_2 (black bar) and O_2 (gray bar) and the selectivity to CO (S_{CO}%, open circles) in the photocatalytic reaction tests with the Ag(*x*)/Pr(1.0,773)/CTO samples, where *x* wt% was (a) 1.0, (b) 2.0, (c) 3.0, (d) 3.5, and (e) 4.0. The values were recorded after 3.5 h photoirradiation.

The photocatalytic activity of the samples in the different loading amount of Ag are shown in Fig. S6. Ranging from 1.0 to 3.5 wt%, the production rate of gas (O_2 and CO) raised gradually with increase of loading. It could be concluded that Ag NPs were still the main active site of CO production in this reaction. When the loading amount of Ag NPs is 4.0 wt%, the yield of gas decreased, but the selectivity to CO still reached 97 % (S_{CO}%). The reason of the decrease may be caused by the agglomeration of Ag.[S1]

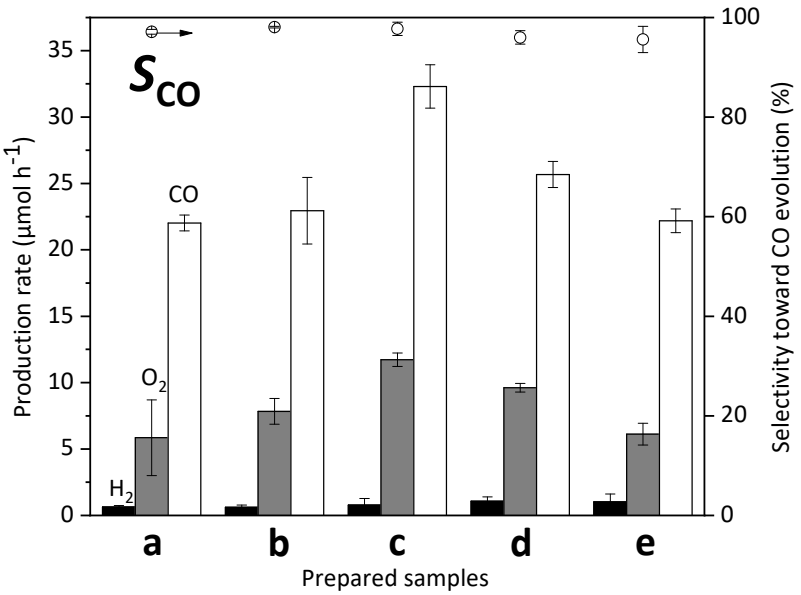

Fig. S7. Formation rates of H_2 (black), CO (white), and O_2 (gray), and the selectivity to CO (S_{CO}%, open circles) in the photocatalytic reaction tests for CO_2 reduction with (a) the Ag(3.5)/CTO sample and the Ag(3.5)/Pr(*y*,773)/CTO samples, where the *y* wt% was (b) 0.5, (c) 1.0, (d) 1.5, and (e) 3.0.

Fig. S8. The GC-MS analysis for the resulting solution after the reaction for 8 h with the Ag(3.5)/Pr(1.0,773)/CTO sample.

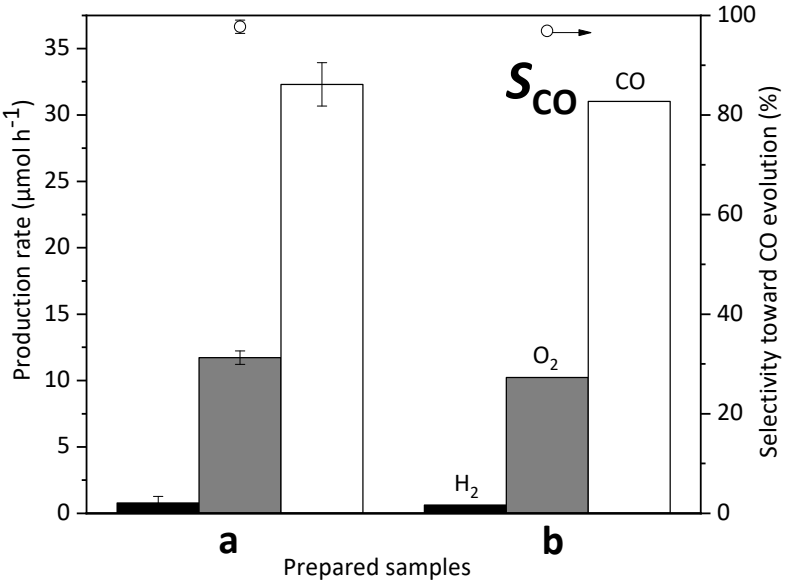

Fig. S9. Formation rates of H_2 (black), CO (white), and O_2 (gray), and the selectivity to CO (S_{CO}%, open circles) in the photocatalytic reaction tests for CO_2 reduction with (a) the Ag(3.5)/Pr(1.0,773)/CTO sample and (b) the used Ag(3.5)/Pr(1.0,773)/CTO sample.

Table S4 Results of the O_2 evolution tests from aqueous solution of $NaIO_3$ (sacrificial reagent). [a]

Entry	Sample	Production rate (μmol h^{-1}) [b]
1	Bare CTO	148.3
2	Pr(1.0,773)/CTO	152.3

[a] Reaction conditions: 0.3 g photocatalyst; 1.5 L deionized water containing sacrificial reagent $NaIO_3$ (5 mM); Ar bubbling rate (30 mL min^{-1}); 400 W high-pressure mercury lamp. [b] The production rates were measured after 2.0 h of photoirradiation.

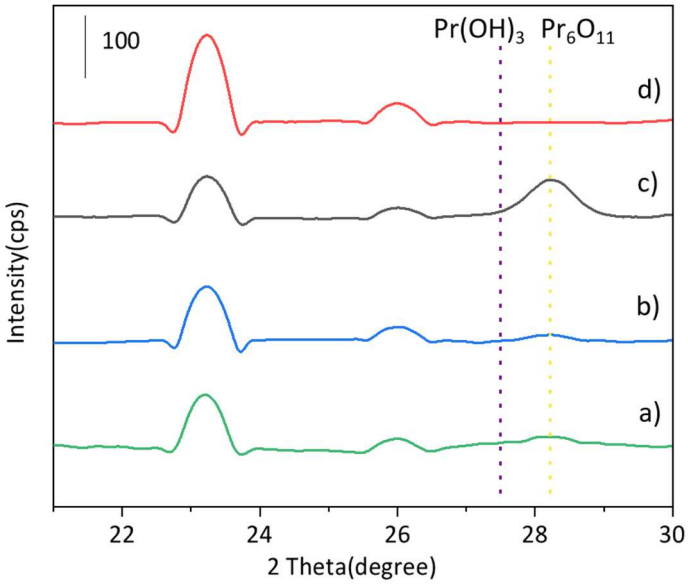

Fig. S10. XRD patterns of (a) the wet Pr(1.0,773)/CTO sample in 1.0 M $NaHCO_3$ which was dispersed in the aqueous $NaHCO_3$ solution with CO_2 flow and filtered; the dried Pr(*y*,773)/CTO samples, where the *y* wt% was (b) 1.0, (c) 10.0, and (d) dried bare CTO sample. The last three samples were dispersed for 5 h in 1.0 M $NaHCO_3$ aqueous solution under a CO_2 flow and dried.

Reference

S1. Anzai, A.; Fukuo, N.; Yamamoto, A.; Yoshida, H., Highly selective photocatalytic reduction of carbon dioxide with water over silver-loaded calcium titanate. *Catalysis Communications* **2017,** *100*, 134-138.